APPLIED ECOLOGY

Global patterns of dust and bedrock nutrient supply to montane ecosystems

Lindsay J. Arvin,[1]* Clifford S. Riebe,[1] Sarah M. Aciego,[1,2] Molly A. Blakowski[2]

Copyright © 2017 The Authors, some rights reserved; exclusive licensee American Association for the Advancement of Science. No claim to original U.S. Government Works. Distributed under a Creative Commons Attribution NonCommercial License 4.0 (CC BY-NC).

A global compilation of erosion rates and modeled dust fluxes shows that dust inputs can be a large fraction of total soil inputs, particularly when erosion is slow and soil residence time is therefore long. These observations suggest that dust-derived nutrients can be vital to montane ecosystems, even when nutrient supply from bedrock is substantial. We tested this hypothesis using neodymium isotopes as a tracer of mineral phosphorus contributions to vegetation in the Sierra Nevada, California, where rates of erosion and dust deposition are both intermediate within the global compilation. Neodymium isotopes in pine needles, dust, and bedrock show that dust contributes most of the neodymium in vegetation at the site. Together, the global data sets and isotopic tracers confirm the ecological significance of dust in eroding mountain landscapes. This challenges conventional assumptions about dust-derived nutrients, expanding the plausible range of dust-reliant ecosystems to include many temperate montane regions, despite their relatively high rates of erosion and bedrock nutrient supply.

INTRODUCTION

Dust can be an important contributor of rock-derived nutrients to ecosystems. In the tropics, for example, where precipitation and temperature are both high, dust inputs can offset nutrient depletion due to intense soil weathering (*1*–*6*). Meanwhile, in arid and semiarid regions, dust from nearby sources can contribute substantially to soils (*7*–*12*) and, moreover, can strongly influence ecosystem phosphorus (P) cycling because dust-derived P inputs tend to be large relative to soil P reservoirs (*13*). Thus, in both wet and dry climates, dust and other sources of atmospheric nutrient deposition (*14*, *15*) can be vital to soil and ecosystem nutrient cycling. This may also be true regardless of climate in eroding landscapes (Fig. 1) (*16*–*18*) if nutrient supply from underlying bedrock is limited by either low bedrock nutrient concentrations (*19*) or slow rock-to-soil conversion rates (*20*). However, the relative magnitude of bedrock and dust inputs has not been quantified across the full range of erosion rates and climatic conditions in Earth's mountain ranges. Moreover, although several studies have quantified uptake of dust-derived nutrients in stable (that is, slowly eroding) landscapes (*3*, *11*, *12*), only a few have done so in montane ecosystems with substantial erosion rates (*6*, *20*). Here, we used global databases of dust fluxes and erosion rates together with Nd isotopic data from one Sierra Nevada study site with moderate rates of erosion and dust deposition to show that dust may provide vital nutrients to many eroding montane ecosystems around the world. Our analysis of global patterns identifies montane ecosystems where the relative importance of dust may be higher than previously thought, whereas our application of isotopic tracers to quantifying nutrient uptake in the Sierra Nevada illustrates how these predictions can be tested on samples of dust, soil, bedrock, and vegetation.

BACKGROUND

To quantify the relative supply of dust and bedrock to an eroding soil (Fig. 1), we use the dust supply index (DSI), defined here as the ratio of dust inputs (D) to the sum of chemical and physical outputs from erosion (E). Because the box model in Fig. 1 explicitly includes erosion, it differs from the conceptual framework for stable (noneroding) soils (*21*), where dust can become increasingly important over time because of progressive nutrient leaching and a lack of fresh mineral supply from bedrock as soils age (*3*). In an eroding soil, the sum of erosional outputs (E) equals the sum of dust and bedrock inputs ($D + B$) in steady state. In that case, DSI, which is calculated as D/E, equals $D/(D + B)$ or f_d, the fraction of soil inputs that are dust-derived. If soil inputs are instead not equal to soil outputs, then DSI will not equal f_d but should still be an indicator of the relative magnitude of dust and bedrock inputs. Furthermore, DSI should be a conservative estimate of the relative contributions of phosphorus from dust and bedrock; the average P concentration

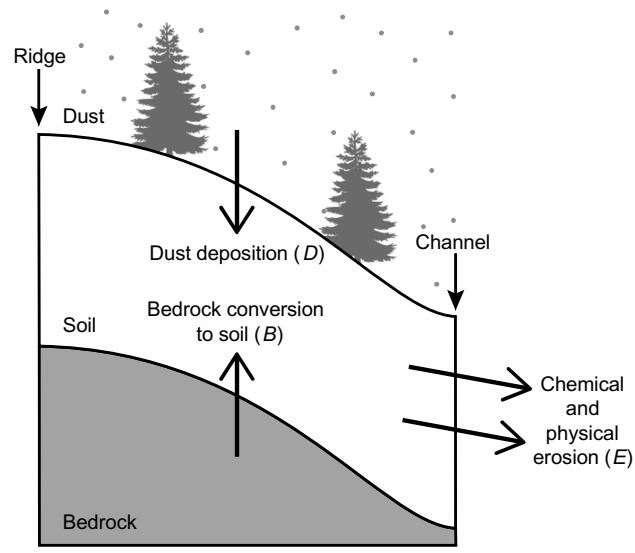

Fig. 1. Fluxes of bedrock and dust in eroding soils. Inputs of soil from dust (D) and bedrock (B) are balanced by outputs from chemical and physical erosion (collectively termed E) on an eroding hillslope. E is a proxy for the sum of inputs from D and B because in steady state, $D + B = E$ and the DSI is equal to f_d. All inputs and outputs reflect total mass flux from both inorganic and organic fractions. Several previous studies have explicitly included dust in the soil mass balance of an eroding hillslope (*16*–*18*). Here, we adopt the conceptual model of Ferrier *et al.* (*18*), which considers net inputs and outputs over an entire watershed (that is, from ridge to channel), consistent with resolution of both the global dust models and the catchment-wide ^{10}Be-based erosion rates.

[1]Department of Geology and Geophysics, University of Wyoming, Laramie, WY 82071, USA. [2]Department of Earth and Environmental Sciences, University of Michigan, Ann Arbor, MI 48109, USA.
*Corresponding author. Email: larvin@uwyo.edu

measured in aeolian dust (*22*) is greater than the median P concentration in a recent compilation of bulk geochemistry from many common rock types (*23*).

Soil erosion rates are now routinely measured at the catchment scale using the cosmogenic nuclide ^{10}Be in sediment (*24*). This has produced a global database of 1149 drainage basins spanning Earth's full range in mean annual precipitation (MAP) and temperature in nearly all possible combinations (*24*). ^{10}Be-based erosion rates include both physical and chemical erosion (and thus quantify *E* in Fig. 1), average over 10^3 to 10^4 years, typically have uncertainties <20%, and are not biased by dust inputs because dust-sized particles are intentionally excluded from ^{10}Be analyses of catchment-wide erosion rates (*25*, *26*). We used reported precipitation data at each site to correct the erosion rates for chemical erosion biases (Materials and Methods), which can lead to systematic underestimation of erosion rates by up to a factor of 2 at temperate and tropical sites, where chemical erosion is significant (*27*).

Dust deposition rates have been directly quantified at many sites but are not often spatially paired with erosion rate measurements (*20*). In lieu of direct observations, we estimated dust deposition rates at each ^{10}Be measurement site using a global dust deposition model (*28*). Dust emission is modeled using estimates of soil moisture, land cover by snow or vegetation, and wind friction velocity; dust transport is estimated using an air advection model; dry dust deposition is calculated from gravitational and turbulent processes; and wet deposition is calculated from a precipitation model (*28*). Modeled dust deposition is therefore based on climate variables and relies on previously developed climate models. Furthermore, the dust deposition model was calibrated with dust flux observations from modern, Last Glacial Maximum (LGM), and interglacial climates. In the synthesis presented here, we queried both the modern and LGM dust deposition models, which should yield minimum and maximum dust fluxes, respectively (*28*, *29*), over the ^{10}Be time scale at most locations (fig. S1).

We combined the ^{10}Be erosion rates with modern and LGM dust fluxes to estimate minimum and maximum bounds on DSI for every drainage basin in the ^{10}Be database. The modeled dust deposition rates have order-of-magnitude uncertainties (*28*), similar to the variability in observed dust deposition rates at the catchment scales of the ^{10}Be database (*30*). However, many of the uncertainties in our estimates of DSI produce conservative (that is, low) estimates of the importance of dust in ecosystem nutrient supply (see Materials and Methods). Moreover, at the global scale, modeled dust deposition rates vary by six orders of magnitude and display coherent patterns that reflect measured dust fluxes in many regions (*28*). Therefore, any global patterns in DSI should reflect regional variations in the relative magnitude of dust and bedrock inputs despite potentially large errors at individual sampling points. To help evaluate these expectations, we supplemented our analyses at the global scale with a focused study of two regions in the ^{10}Be database where both long- and short-term average erosion rates are available at the catchment scale. This allowed us to compare observations across time scales and thus evaluate how the relative importance of dust and bedrock in the production of soil can change over time.

To determine whether inputs of dust can have a significant effect on montane ecosystems, we used Nd isotopes to trace nutrient uptake by vegetation at one of our study sites. Nd isotopes are promising tracers of P because rare earth elements (REEs) such as Nd and Sm tend to be concentrated in phosphate-bearing minerals (*3*). The uptake of dust-derived Nd by plants should therefore reflect the weathering of dust-derived phosphate minerals and the subsequent contribution of dust-derived mineral P to the ecosystem. This approach builds on previous applications of Nd isotopes for tracing dust-derived P inputs to soils (*3*). It differs from and complements strontium-based methods for gauging plant uptake of alkaline earth elements such as Ca and Mg (*3*, *11*, *12*, *31*). Nd isotopes have rarely been measured in vegetation because of difficulties in measuring isotope ratios in Nd-poor materials such as biomass. We overcame the limitation of low Nd concentrations in plant tissues using high-pressure microwave digestion and high-precision thermal ionization mass spectrometry (*32*). By focusing on the Providence dust collection site, we also capitalized on previously published direct measurements of Nd isotopes in locally collected dust (*20*), which is not often available. Strontium isotopes in the bulk (inorganic and organic) dust have shown that it is derived from both regional and transoceanic sources (*20*).

RESULTS AND INTERPRETATION

Our estimates of DSI range from 7×10^{-4} to 20 for the LGM dust fluxes, and from 1×10^{-5} to 8 at present in the global database [Fig. 2 and table S1; (*33*, *34*)]. The difference in range reflects the markedly higher modeled dust fluxes during the LGM, particularly in Europe, southern South America, and eastern North America (Fig. 2 and fig. S1) (*28*). Despite large uncertainties in modeled dust deposition rates, our estimates of DSI are consistent with previously recognized patterns of dust inputs. For example, our estimates of DSI from the modern dust model are relatively high at many sites with low MAP because of the proximity of these sites to arid regions with high modeled dust emissions (*28*). This is consistent with modern observations of the importance of dust in arid and semiarid ecosystems (*7*–*13*) (Fig. 2C). Additionally, average DSI at temperate sites is more than 30 times higher for LGM versus modern dust fluxes (table S1). For example, LGM-based estimates of DSI exceeding 0.5 in the eastern United States and Western Europe (Fig. 2) partly reflect high regional dust fluxes (fig. S1). This is consistent with rapid glaciogenic dust production in continental interiors during the LGM (*35*) and results from the explicit consideration of glaciogenic dust source areas in the dust deposition model (*28*).

High dust fluxes in the LGM are only part of the reason for the higher DSI in the eastern United States and Western Europe. An additional cause is slow erosion in the eastern United States (mean, 0.02 mm year^{-1}) and nonalpine Western Europe (mean, 0.05 mm year^{-1}) relative to the global data set (mean, 0.2 mm year^{-1}) (table S1). At these slowly eroding sites, high dust inputs are an even larger fraction of total soil input than they would be at more rapidly eroding sites.

Although dust fluxes in the eastern United States and Western Europe have subsided substantially since the LGM (fig. S1), slow erosion rates and long soil residence times in these regions imply that high LGM-based DSI estimates are relevant to modern ecosystems (Fig. 3). For example, a 1-m-thick soil will have a residence time of 50,000 years if the erosion rate is 0.02 mm year^{-1}, a typical condition in the eastern United States (see Materials and Methods and table S1) (*36*). This demonstrates that soils with slow erosion rates can have residence times spanning glacial-interglacial time scales (Fig. 3 and fig. S2), making them integrative of both modern and LGM dust fluxes. This suggests that past dust fluxes (for example, during the LGM) may be particularly relevant to slowly eroding sites, where DSI tends to be high and where soil residence times are relatively long. Sites with slow erosion rates have high DSI values because *E* is the denominator of DSI, but the lack of correlation between dust fluxes and erosion rates (Fig. 3C) suggests that these two factors contribute roughly equally to high DSI values in the LGM.

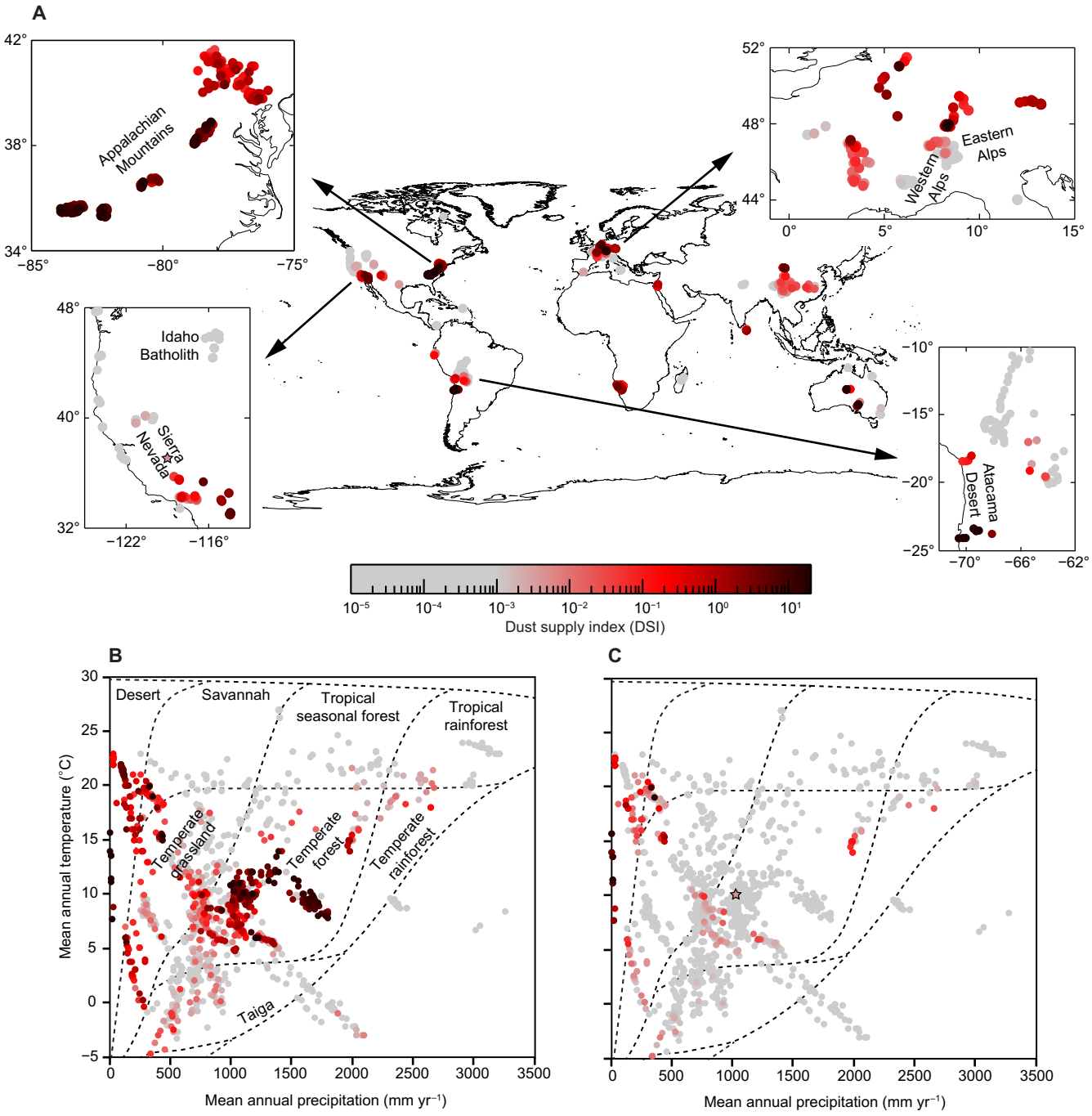

Fig. 2. The DSI in mountain catchments around the world. (**A**) DSI calculated from a compilation of ^{10}Be-based erosion rates (*24*) and a global model of LGM dust fluxes (*28*). (**B**) DSI from (A) in relation to modern MAP and mean annual temperature (MAT) for each sampling location, with modern biomes delineated by dashed lines [after the work of Whittaker (*33*)]. (**C**) Same as (B) except that DSI is inferred using modern instead of LGM dust fluxes. The star indicates a DSI of 0.15 calculated from direct observations of dust fluxes and ^{10}Be-based erosion rates in the southern Sierra Nevada, California (*20*, *34*). The uncertainty in individual DSI estimates is approximately an order of magnitude due to the order-of-magnitude uncertainty in dust deposition rates (*28*).

For a more focused perspective on relative dust inputs, we quantified DSI in two regions from the ^{10}Be database where the long-term average erosion rates from cosmogenic nuclides are supplemented by direct observations of sediment yields, which average over time scales commensurate with the modeled modern dust flux and have been corrected to account for both chemical and physical erosion (see Materials and Methods). We can therefore calculate modern values of DSI that reflect modern erosion rates and compare them to LGM-based values of DSI that reflect long-term average erosion rates. Across 32 catchments in central Idaho, modern DSI estimates are 35% higher on average than LGM-based DSI estimates despite a 10-fold decrease in modeled dust inputs to the catchments from the LGM to the present (table S2 and fig. S3). This is explained by the even larger difference between long-term and short-term erosion rates, a discrepancy that is thought to

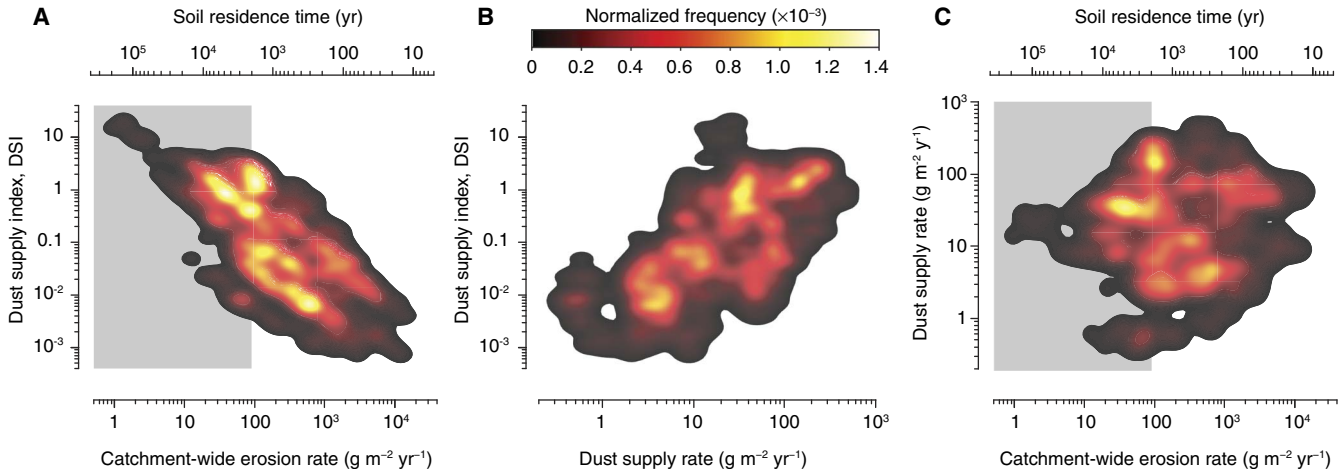

Fig. 3. Soil residence times, dust fluxes, and DSI from the global database. (**A**) Bivariate density plot of DSI and catchment-wide erosion rates. Here, DSI is calculated from ^{10}Be-based erosion rates (*24*) and LGM dust fluxes (*28*). It is commonly higher at sites with longer soil residence times, calculated for a 1-m-thick soil with a density of 1.8 g cm^{-3} (see Materials and Methods). The gray region marks estimated residence times that are greater than or equal to 20,000 years, highlighting instances where soils may harbor legacies of dust accumulation from the LGM, when fluxes were much higher than they are today. (**B** and **C**) DSI is also high at sites with high dust input rates, and there is little correlation between rates of erosion and dust deposition. Together, these observations suggest that erosion rates and dust input rates contribute roughly equally to observed global patterns in DSI.

reflect contributions of large infrequent erosion events to the long-term averages (*37*).

The pattern of relatively high modern DSI estimates despite relatively low modern dust deposition rates is not restricted to a single site. This pattern is even more pronounced in the southern Sierra Nevada, where short-term erosion rates are two orders of magnitude slower than long-term erosion rates on average across eight catchments (see Materials and Methods and table S2). Because of this large, time scale–related difference in erosion rates, modern DSI values from sediment yields are 50% higher on average than LGM-based DSI values (0.19 versus 0.13), although modern dust inputs are only 4% of LGM dust inputs to these catchments (Fig. 4) (*38*).

Our analysis of DSI patterns suggests that dust-derived nutrients are important to many montane ecosystems around the world (Figs. 2 and 3). To test this hypothesis, we used Nd isotopes (ε_{Nd}) in dust, bedrock, soil, and pine needles to estimate the relative contributions of dust- and bedrock-derived mineral P. We focused on trees near the Providence dust collection site in the southern Sierra Nevada (see Fig. 4 for location), where DSI estimates from direct observations (0.15) and LGM dust fluxes (0.13) are moderate relative to the global compilation, implying that it should be comparable to many eroding mountain sites.

To quantify the relative contributions of dust and bedrock to Nd supply in soils, we measured Nd isotopic ratios in soils and bedrock samples from a nutrient-poor granitic pluton (*34*) near the Providence dust collection site. Using a two-component mixing model of bedrock and dust (see Materials and Methods and tables S3 and S4), we find that 77 ± 6% (mean ± SEM) of Nd in the soil is dust-derived (Fig. 5). Furthermore, we used measured concentrations of Nd in dust and bedrock to convert from the proportion of Nd in the soil that is dust-derived to the proportion of total soil that is dust-derived (*18*). We find that 90 ± 4% of the soil is dust-derived.

To quantify the contribution of dust to vegetation, we measured Nd isotopes in *Pinus jeffreyi* pine needles and found that 88 ± 7% of Nd in the pine needles is dust-derived (Fig. 5 and tables S3 and S4). Assuming that P uptake is directly reflected by Nd uptake, we estimated that >99% of P in the pine needles is dust-derived (see Materials and Methods). However, more work is needed to evaluate this assumption and to demonstrate the extent to which Nd serves as a proxy for P cycling in soil and vegetation. Nevertheless, our finding that dust-derived Nd contributes substantially to Nd pools in both soil and biomass suggests that dust provides vital nutrients to the Sierra Nevada ecosystem.

DISCUSSION

Some minerals are more easily weathered than the bulk rock in near-surface environments (*39*). This can lead to incongruent weathering that confounds inferences from tracer analyses if the isotopic ratios of the minerals differ from the bulk rock. For example, accessory minerals that contain much of the Nd in granitic bedrock tend to have higher Sm/Nd ratios, and therefore higher ε_{Nd} signatures, than bulk rock (*40*, *41*). In addition, some of these minerals, including the P-bearing mineral apatite (*42*), are more easily weathered than the bulk rock, so the ε_{Nd} released to plants by bedrock weathering may be higher than the ε_{Nd} signature of bulk rock. If this is the case, then the ε_{Nd} that we used for the bedrock source in our mixing calculations (Fig. 5) may be too low and the estimated fraction of dust-derived Nd in vegetation may be too high. To determine whether this is the case, we used data from the literature (*40*, *43*) to calculate the potential ε_{Nd} contrast between readily weathered minerals apatite, biotite, and sphene and the bulk rock. On the basis of these calculations, we estimate that bulk rock differs from nutrient sources for trees by 1 ε unit at most, which suggests that at least 84% of Nd and >99% of P in the pine needles is dust-derived (see Materials and Methods), consistent with interpretations outlined earlier.

Our $f_{d,Nd}$ calculation assumes that the dust collection, which integrates over months (*20*), represents Nd isotopic contributions over the time scale of soil formation. It is possible that shifting proportions of dust from the two known source areas, the Central Valley and the Gobi Desert, could cause the Nd isotopic composition of dust to vary over time. However, shifting proportions of dust from these two source areas could only result in a lower ε_{Nd} value for dust inputs over time because ε_{Nd} in the two dust source areas is less than or equal to the modern dust ε_{Nd} (*20*). If ε_{Nd} values for dust deposited near the Providence

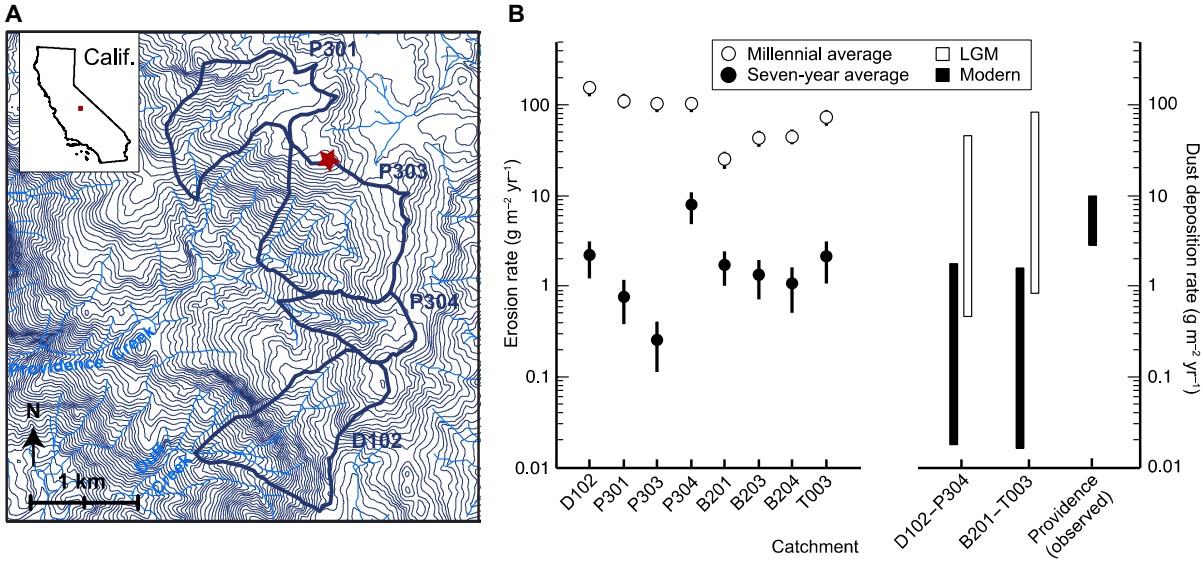

Fig. 4. Erosion rates and dust fluxes in the southern Sierra Nevada, California. (**A**) Four southern Sierra Nevada catchments where erosion rates have been measured by both ^{10}Be and sediment yields. The star indicates the location of the Providence dust collection site in the study of Aciego *et al.* (*20*). (**B**) ^{10}Be-based erosion rates (see Materials and Methods), sediment yield-based erosion rates (*38*), and modeled LGM and modern dust fluxes (*28*) for eight southern Sierra Nevada catchments. Observed dust deposition rate from the Providence dust collection site is also displayed. P concentration in dust collected at the Providence dust collection site is 2.5 times greater than the average P concentration in local bedrock (*20*), suggesting that the modeled DSI is underestimated at this site. Error bars reflect propagated analytical uncertainty in ^{10}Be-based erosion rates and SEM of seven measurements for sediment yield-based erosion rates. The range for dust fluxes represents order-of-magnitude uncertainty in modeled dust fluxes and observed range in measured dust fluxes at the dust collection site (*20*).

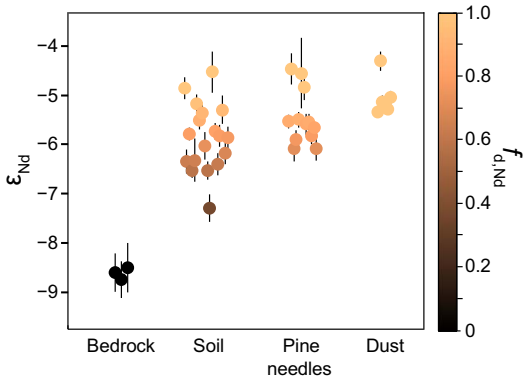

Fig. 5. Nd isotopes reveal plant utilization of dust-derived nutrients. ε_{Nd} measurements in bedrock, soil, and pine needles are combined with ε_{Nd} measured in dust collected nearby (Fig. 4) in previous work (*20*). $f_{d,Nd}$ reflects the fraction of Nd that is dust-derived based on a two-component isotopic mixing model. Errors bars show internal reproducibility (1 SD).

dust collection site were lower in the past than ε_{Nd} values in modern times, then our estimate of the dust-derived Nd contribution to soils is a minimum and therefore conservative relative to our interpretations. Moreover, given that dust and bedrock should bracket soil in their Nd isotopic ratios, ε_{Nd} in dust inputs must be greater than the soil ε_{Nd} values, which are only slightly lower than ε_{Nd} in the collected dust (Fig. 5), implying that errors due to variations in Nd sources over time are likely small.

The discrepancies between LGM and modern DSI patterns (Fig. 2, B and C) may be explained in part by mismatches in time scale between erosion rate and dust flux measurements. Thus, our analysis of global patterns of DSI highlights another way that nonsteady fluxes could lead to misinterpretation of the role of dust in ecosystems. The same millennial average ^{10}Be erosion rates are used in both the LGM and modern estimates of DSI, whereas the modeled dust fluxes represent markedly different conditions (that is, LGM versus modern climate) at Earth's surface. In general, dust fluxes are much slower now than during the LGM. However, low modern dust fluxes may still contribute a large fraction of soil inputs over short time scales in regions where episodic erosion makes short-term average erosion rates slower than long-term rates. Thus, low modern dust inputs may promote the false assumption that the fractional contribution of dust to soil and its importance to the ecosystem are low. Our analysis of the central Idaho and Sierra Nevada study areas (Fig. 4 and fig. S3) shows that these assumptions can be tested using short-term average erosion rates. However, these measurements are rare in catchments that are not complicated by sediment storage (for example, in dams and floodplains) and other factors that might confound comparison of dust- and bedrock-derived nutrient fluxes using the simple box model of Fig. 1.

Observations from central Idaho and the Sierra Nevada suggest that modern and LGM-based DSI estimates are roughly similar, differing by less than 0.08 in Idaho, for example, because differences in erosion rates are offset by differences in dust fluxes over time (fig. S3). However, DSI can provide insight into ecosystem nutrient cycling over either time scale even when modern and LGM-based estimates disagree. For example, if infrequent erosion episodes make the long-term average erosion rate much larger than the short-term average (*37*), then DSI calculated from sediment yield data can provide a temporally matched benchmark for comparison with modern dust fluxes. These modern DSI values should therefore reflect the relative importance of dust over the short term.

The inference that high LGM dust fluxes can continue to influence modern soils because of long residence times in slowly eroding landscapes (Fig. 3) may have implications for understanding nutrient cycling in modern ecosystems in the eastern United States and Western Europe:

Soil P turnover of dust inputs (*13*) is longer than estimated soil residence times in these regions (table S1), suggesting that paleo dust inputs from the LGM can persist as a nutrient source in modern soils. Conversely, at more rapidly eroding sites (for example, in the Himalaya), soil residence times are less likely to span glacial-interglacial time scales, especially if soils are also thin, and soil inputs are more likely to be dominated by bedrock. Our analysis of soil residence times (Fig. 3) therefore highlights a previously underappreciated pitfall of using modern dust fluxes to study integrated effects of dust on modern soils, especially in regions with slow erosion rates and high glaciogenic dust fluxes in the LGM.

Given that DSI at the Providence site is intermediate compared to other sites in our global compilation (Fig. 2 and table S1), the Nd isotopic evidence of high dust contributions to soil and biomass supports the hypothesis that many montane ecosystems around the world receive vital nutrient subsidies from dust. The nutrient-poor granite of our Nd study site (*34*) may accentuate the importance of dust for this ecosystem; additional data are needed to evaluate how ecosystem nutrient status affects the importance of dust-derived nutrients at other montane sites. Our results challenge the conventional assumption that dust is relatively unimportant in mountain landscapes where bedrock conversion to soil provides continuous nutrient supply to ecosystems. Furthermore, our analyses demonstrate the potential to investigate the importance of dust in montane ecosystems at multiple spatiotemporal scales. For example, our global synthesis of erosion rates and dust fluxes highlights ecosystems that may be more strongly influenced by dust than previously recognized (Fig. 2), and our application of Nd isotopic measurements from bedrock, dust, and vegetation demonstrates a tool for determining whether this is the case at individual sites (Fig. 5). However, more work is needed to identify other montane sites where dust plays a vital role in ecosystem nutrient cycling and thus evaluate whether the Sierra Nevada results are consistent with other montane ecosystems where DSI is moderate to relatively high.

MATERIALS AND METHODS

Global DSI compilation

We used a published database of 1393 ^{10}Be-based erosion rates from 1149 drainage basins that span the globe (*24*). In this data set, there were 1306 unique sampling locations (because some sampling locations had replicate samples). At each sampling location, we extracted dust deposition rates recorded in units of grams per meter squared per year from models of both modern and LGM conditions (*28*) (fig. S1 and table S1). The erosion rates and dust deposition rates from the data compilation were used to calculate two estimates of DSI at each site: one based on the LGM dust deposition rate and one based on the modern dust deposition rate (table S1). In the text, we report average erosion rates for the eastern United States and nonalpine Western Europe that were calculated from the ^{10}Be database for sites within the following coordinates: 30° to 45°N and 70° to 90°W for the eastern United States and 48° to 60°N and 10°W to 20°E for nonalpine Western Europe.

The buildup of cosmogenic nuclides in minerals eroded to the surface reflects the loss of mass from overlying soil and weathered rock due to chemical and physical erosion (*44*). Thus, cosmogenic nuclide concentrations record erosion rates in units of mass per area per time (*45*). However, the CRONUS-based (*46*) erosion rates in the ^{10}Be database were reported in units of length per time (*24*). Although this is common in the geomorphology literature, it requires a unit conversion, typically using bedrock density, which yields estimates of bedrock lowering rates [reported in meters per million years by Portenga and Bierman (*24*)]. To quantify DSI, which we conceptualize as a dimensionless ratio of the relative flux of dust (Fig. 1), we needed the erosion rates of the ^{10}Be database in their original M (mass) L (length)$^{-2}$ T (time)$^{-1}$ dimensions to make them consistent with units reported in the dust models. We therefore converted the erosion rates into units of grams per meter squared per year using a bedrock density of 2.7 g cm^{-3} unless a different density was provided, consistent with the densities used in the original compilation (*24*).

All ^{10}Be-based erosion rates used in this study were corrected for the chemical erosion bias recognized in previous work (*27*, *47*–*49*); we calculated the predicted chemical erosion factor (CEF) at each site based on MAP (*27*), which is provided for each site in the database, and used it to correct each ^{10}Be-based erosion rate (tables S1 and S2). Although the relationship used in the CEF corrections is based on observations from just 10 sites and therefore has considerable uncertainties (*27*), the theory behind the chemical erosion bias has been recognized for nearly two decades (*27*, *47*–*49*); failure to account for it at sites with differing chemical weathering can lead to systematic underestimation of erosion rates by up to a factor of 2 (*27*). Thus, our estimates of DSI are lower than they would be if we ignored the chemical erosion bias, and our conclusions about the potentially widespread importance of dust in montane ecosystems are therefore conservative with respect to our decision to use CEF-corrected erosion rates. Moreover, because CEF increases systematically with precipitation (*27*), it is larger and therefore more conservative about DSI at the potentially dust-reliant temperate montane sites highlighted in our analysis, at least compared to arid sites where dust inputs are already recognized to be important.

To estimate soil residence times for table S1 and Fig. 3, we used a 1-m-thick soil, which is typical in many mountain catchments [see, for example, the work of Wald *et al.* (*36*)], and assumed a soil density equal to 1.8 g cm^{-3}, consistent with mineral-rich mountain soils. Residence time is equal to soil mass (that is, the product of soil thickness and soil density) divided by soil erosion rate. The soil erosion rate is the sum of both physical and chemical losses from the soil. Because our CEF correction includes deep (saprolite-derived) chemical erosion losses (*27*) that cannot be confidently separated from chemical erosion in overlying soil, the CEF-corrected erosion rates in table S1 may overestimate soil erosion rates by as much as 20% at sites where deep losses are significant (*27*). This should yield soil residence times that are conservative relative to our conclusions about the previously underappreciated importance of LGM dust fluxes at temperate sites with deep weathering (Fig. 3). Furthermore, soil residence times are likely underestimated in slowly eroding regions (including the eastern United States, where DSI is also relatively high), because more slowly eroding soils tend to be thicker (*50*). Thus, although the soil residence times shown in Fig. 3 require several, difficult-to-confirm assumptions about soil thickness, soil density, and soil erosion rate, they should be mostly conservative to the extent that they demonstrate the potential for LGM influence on soils in the global compilation.

Central Idaho erosion rates

For the case study of central Idaho (Fig. S3 and table S2), ^{10}Be-based erosion rates and sediment yields were compiled from published data sets (*24*, *37*). ^{10}Be-based erosion rates were measured from stream sediment at locations where sediment yields were also measured (*37*). However, we used ^{10}Be-based erosion rates from the global compilation (*24*) rather than originally reported values (*37*) and thus incorporated corrections needed to account for revisions made roughly 10 years ago to the ^{10}Be half-life (*51*). ^{10}Be-based erosion rates were adjusted for predicted

CEF (*27*), as described in the previous section. Sediment yield measurements (*37*) were adjusted to include chemical as well as physical erosion using chemical depletion fractions (CDFs) predicted from the denudation rate (assumed here to be the chemical erosion–corrected ^{10}Be-based erosion rate), the MAP, and the MAT at the site using a previously published predictive formula that was calibrated using data from 42 climatically diverse sites (*52*).

Southern Sierra Nevada erosion rates

For the case study of the southern Sierra Nevada (Fig. 4 and table S2), we compiled published sediment yield measurements (*38*) with new ^{10}Be-based erosion rates for each catchment in the sediment yield data set. For catchments D102, P301, P303, and P304, we used published ^{10}Be concentrations (*34*) but recalculated the ^{10}Be-based erosion rates to account for recent advances in calculating topographic shielding (*53*). For catchments T003, B201, B203, and B204, we measured new ^{10}Be concentrations, which we used to calculate ^{10}Be-based erosion rates using standard methods (see the succeeding sections for details). Sediment yield measurements were adjusted by a predicted CDF (*52*), and ^{10}Be-based erosion rates were adjusted by a predicted CEF (*27*), consistent with methods described in previous sections.

Central Idaho and southern Sierra Nevada DSI

We extracted modeled modern and LGM dust deposition rates at the sampling location of each catchment. For very large catchments, this may introduce error if modeled dust deposition is not uniform across the area. However, these errors are likely small in our study; the modeled dust deposition rates do not show large spatial variations across the central Idaho and southern Sierra Nevada study sites, and the spatial resolution of the dust deposition model is such that most study basins fall within a single dust deposition rate value. Modern DSI estimates were calculated for each catchment using modern dust deposition rates and sediment yield measurements adjusted according to protocols described above. LGM-based DSI estimates were calculated for each catchment using LGM dust deposition rates and CEF-adjusted ^{10}Be-based erosion rates (table S2).

Sample preparation and analyses of ^{10}Be in quartz

In addition to the 1149 basins in the ^{10}Be data compilation, we also reported ^{10}Be-based erosion rates from eight catchments in the Sierra Nevada Critical Zone Observatory. Four of these erosion rates (from catchments D102, P301, P303, and P304) were based on data published in previous work (*34*). The other four (from catchments T003, B201, B203, and B204) were based on stream sediment samples collected and analyzed for ^{10}Be as part of this work.

We separated quartz from sediment using standard techniques (*54*, *55*) and then spiked quartz separates with ^{9}Be, dissolved it, and extracted Be in University of Wyoming analytical facilities following standard procedures. ^{10}Be/^{9}Be ratios were measured by accelerator mass spectrometry (AMS) at the Purdue Rare Isotope Measurement Laboratory (*56*). Process blanks typically had ^{10}Be/^{9}Be ratios $<1 \times 10^{-14}$. We used the AMS data to calculate ^{10}Be concentrations in quartz. Results are reported in table S2.

Calculating erosion rates from ^{10}Be data

We used the newly developed CAIRN (Catchment-Averaged denudatIon Rates from cosmogenic Nuclides) method (*53*) to calculate erosion rates from the four original ^{10}Be concentrations (catchments T003, B201, B203, and B204) and to recalculate erosion rates for four previously published ^{10}Be concentrations (catchments D102, P301, P303, and P304). We used an established muogenic scaling scheme (*57*), derived snow shielding from a local relationship between snow-water equivalent and elevation (*58*) (available at http://cdec.water.ca.gov), and corrected for biomass shielding using average canopy cover (*59*). The CAIRN method differs from previous methods for calculating erosion rates (*46*) in that it calculates topographic shielding and cosmogenic nuclide production for each individual pixel within a catchment rather than the average elevation of the catchment (*53*).

Sample collection for Nd isotopic analysis

Bedrock, soil, and pine needles were sampled from the Bald Mountain Granite in the southern Sierra Nevada, California, at locations between 37.126° and 37.131°N and between 119.189° and 119.192°W. This sampling area was selected because previous work has shown that primary productivity atop the Bald Mountain Granite may be limited by low bedrock nutrient concentrations (*34*) and because the ecosystem appears to be experiencing dust nutrient inputs that are on par with bedrock nutrient inputs (*20*). If dust plays a significant role in nutrient supply to vegetation in the southern Sierra Nevada, then it should be evident at this site. The dust samples and dust Nd isotopic data used in the analyses presented here were collected in previous work by several of this study's coauthors (*20*) at the Providence dust collection site (see Fig. 4).

Three fresh bedrock cores were sampled from the Bald Mountain Granite using a water-cooled Pomeroy rock drill with a 10.2 cm bit. Pine needles were sampled from 13 different mature *P. jeffreyi*, which is one of the dominant tree species at the site. Small portions of four to five branches were cut from each tree using a tree pruner, and pine needles were torn from the branches with an effort to homogenize pine needle age and position. The soil mantle at the study site is discontinuous, and all soil sampling locations corresponded to localized soil pits surrounding mature trees. The A horizon of soil was sampled within 2 m of each sample tree, and the B horizon of soil was sampled at the same location if it was present. Soil Nd isotopic measurements included both organic and inorganic fractions.

Sample preparation for Nd isotopic analysis

Bedrock samples were crushed and then powdered using a tungsten carbide grinding pot in a SPEX brand Shatterbox. Soil samples were dried before being powdered in the Shatterbox. Pine needle samples were dried and then ashed in a muffle furnace in ceramic crucibles. Crucibles were precleaned in an overnight bath of 7 N trace metal grade HNO_3 and rinsed in 18.2 megaohm·cm water. During ashing, the muffle furnace was heated from room temperature to 500°C over the course of 2 hours and then kept at 500°C for an additional 8 hours.

All preparation and analysis for Nd isotopic ratios were performed in a class 10,000 clean room at the University of Michigan. Sample digestion methods varied between the needles and the soils. Pine needles were dissolved using a closed-vessel high-pressure microwave-accelerated acid cocktail, with 2 g of powdered needles weighed into each 100-ml Teflon digestion vessel. Concentrated nitric acid (10 ml; 65% Seastar) and 30% hydrogen peroxide (0.5 ml; Optima) were added to the vessel, and the mixture was digested using the following program: stage 1: ramp to 690 kilopascals (kPa) over 5 min, hold at 690 kPa for 5 min; stage 2: ramp to 1380 kPa (5 min) and hold for 10 min; stage 3: ramp to 2410 kPa (2.5 min) and hold for 25 min. After coming out of the microwave, samples were treated three times in the following manner: dried, dissolved in 2 ml of 7 M HNO_3 + 0.1 ml of H_2O_2, capped overnight, and warmed on a hot plate at 90°C.

For the soil and bedrock samples, approximately 10 to 20 mg of sample was weighed into 3-ml Teflon beakers. These were pretreated with two dry-downs in 1 ml of 16 M HNO_3 + 1 ml of 25 M HF + 0.5 ml of Optima H_2O_2 at ~110°C; however, some of the garnet- and zircon-bearing samples remained cloudy or yielded precipitates after the second dry-down and therefore required up to four dry-downs to eliminate fluorides. Following advice in previous work (*60–62*), we dissolved the pretreated soils in highly pressurized, steel-jacketed Parr bombs via a two-phase acid attack. For the initial digestion, samples were brought up in concentrated hydrofluoric acid, sealed in the polytetrafluoroethylene-lined Parr bomb, and placed in an oven set to 220°C for 48 hours. Samples were then dried down and exposed to a shorter (16 to 24 hours) phase in 6 M HCl at 180°C to complex any fluorides remaining after the first attack. Following the second digestion, it was ensured that dissolution treatments yielded a clear, fully dissolved solution.

Digested pine needle, soil, and bedrock solutions were dried down, brought back up in 1 ml of 9 M hydrochloric acid, and then split: 10% for elemental analysis by inductively coupled mass spectrometry (ICP-MS) and the remainder for ion exchange chromatography and subsequent radiogenic isotope analysis, using column chromatography methods established elsewhere (*20*) to isolate Nd.

Nd isotopic analyses

Samples reserved for isotopic analysis were loaded into columns filled with 50- to 100-μm mesh TruSpec resin, splitting each sample into three cuts. The second cut, which contained the REEs and the high–field strength elements (HFSEs), was set aside for further Nd column chemistry. REEs in this cut were separated from HFSE by loading the samples into columns filled with 100- to 200-μm LnSpec resin. Nd was isolated from the REE cut by loading the REE cut into columns containing 50- to 100-μm LnSpec resin and exposing the samples to a sequence of hydrochloric acids of varying normality (*63*). The isolated Nd cuts were dried down and then brought back into solution by 1 ml each of 3 M HCl and 3 M HNO_3.

The isolated Nd solutions were loaded onto outgassed rhenium double filaments. A current of 0.8 A was run through the filament until the sample dried, and then the current was increased to 1.8 A, held for 60 s, and then flashed at 2.2 A before returning to 0 A. Isotopic ratios were measured using a Thermo Scientific Triton PLUS thermal ionization mass spectrometer in the Glaciochemistry and Isotope Geochemistry Laboratory at the University of Michigan, following methods detailed elsewhere (*64*). Nd was normalized to $^{146}Nd/^{144}Nd = 0.7129$ to correct for mass fractionation, and mass 149 was monitored for Sm interference.

The Nd isotopic standard JNdi-1 (10 ng) yielded $^{143}Nd/^{144}Nd = 0.512090$ ($2\sigma = 1.0 \times 10^{-5}$), whereas the Columbia River Basalt (BCR-2) United States Geological Survey rock standard processed along with the samples used in this work was measured to have a $^{143}Nd/^{144}Nd$ ratio of 0.512624, or $\varepsilon_{Nd} = 0.35$ ($2\sigma = 0.67$). Measured blanks were considered to be negligible. Our results are reported in terms of their deviations from the Chondritic Uniform Reservoir (CHUR) evolution line, wherein $\varepsilon_{Nd}(0) = ((^{143}Nd/^{144}Nd)_{meas}/(^{143}Nd/^{144}Nd)_{CHUR}) - 1) \times 10^4$, using the present-day CHUR value of 0.512638 defined in previous work (*65*).

P and Nd elemental analyses

The 10% elemental splits for the three bedrock samples were dried and redissolved in 10 ml of 5% HNO_3, with which analyses were performed on a PerkinElmer SCIEX ICP-MS at the University of Colorado Boulder to determine P/Nd ratios (table S5). Indium was used as an internal standard. Four standards (blank, 100, 500, and 1000 parts per billion) were used for calibration.

Mixing calculations

The fraction of Nd in soil and in pine needles that is dust-derived ($f_{d,Nd}$) was determined using a two-component mixing model between dust and bedrock. Analytical errors from measuring ε_{Nd} and errors in estimating mean ε_{Nd} values were propagated to determine SEs of each mean (bedrock, soil, pine needles, and dust), and Gaussian error propagation was used to determine the error in estimated $f_{d,Nd}$ values (table S4). The fraction of total soil that is dust-derived (f_d) was calculated from $f_{d,Nd}$ of soil and end-member Nd concentrations (table S6) using the following equation

$$f_d = [Nd]_{rock} \times f_{d,Nd} / ([Nd]_{dust} \times (1 - f_{d,Nd}) + [Nd]_{rock} \times f_{d,Nd})$$

Here, brackets denote concentrations. Errors were propagated by bootstrapping using a Monte Carlo approach. The fraction of P in pine needles that is dust-derived was calculated from $f_{d,Nd}$ of pine needles and end-member Nd and P concentrations (table S6) using the estimate of f_d from above and the following equation

$$f_{d,P} = [P]_{dust} \times f_d / ([P]_{dust} \times f_d + [P]_{rock} \times (1 - f_d))$$

Dust Nd and P concentrations were previously published (*20*). Bedrock Nd concentrations were not available, but bedrock P concentrations were previously published (*34*), and we estimated bedrock Nd concentrations on the basis of our quantification of P/Nd ratios in three bedrock samples analyzed here (table S5).

Incongruent weathering effect on bedrock ε_{Nd}

To gauge the potential effects of incongruent weathering on our analysis of Nd uptake by vegetation, we used Sm/Nd values for bulk granite and constituent apatite, biotite, and sphene to calculate their ε_{Nd} composition over time (*40*, *43*). We used CHUR as the initial ratio and a conservative age of 100 million years (My) for the Bald Mountain Granite (*66*). We calculated the ε_{Nd} evolution over time using a standard radioactive decay relationship with a decay constant of 6.54×10^{-12} years for ^{147}Sm. The offset after 100 My is just 1 ε unit for Sm/Nd ratios of 0.162 in bulk rock and 0.241 in apatite, based on data from a Japanese granite (*43*). Following the study of Gromet and Silver (*40*), which reports data from southern California, we also calculated offsets using Sm/Nd ratios of 0.104 in granite, 0.106 in apatite, 0.129 in biotite, and 0.147 in sphene: The calculated offset is 0.5 ε units for sphene, 0.3 for biotite, and negligible for apatite. We used the highest of these plausible offsets (1 ε unit) to adjust bedrock ε_{Nd} to −7.61 and then used it to calculate an $f_{d,Nd}$ of 0.84 for the pine needles, a difference of just 5% from the estimate reported in the text (see table S4).

SUPPLEMENTARY MATERIALS

Supplementary material for this article is available at http://advances.sciencemag.org/cgi/content/full/3/12/eaao1588/DC1

fig. S1. Combination of existing global data sets.

fig. S2. Systematically higher DSI in soils with longer residence times.

fig. S3. Comparison of LGM-based DSI estimates and modern DSI estimates in Idaho.

table S1. Global DSI estimates from ^{10}Be-based erosion rates (*24*) and global models of modern and LGM dust fluxes (*28*).

table S2. DSI estimates for the southern Sierra Nevada and central Idaho.
table S3. Nd isotopic measurements (ε_{Nd}) of southern Sierra Nevada bedrock, soil, and pine needles.
table S4. $f_{d,Nd}$ for southern Sierra Nevada soils and pine needles.
table S5. P/Nd ratios of southern Sierra Nevada bedrock.
table S6. P and Nd concentrations of southern Sierra Nevada dust and bedrock.

REFERENCES AND NOTES

1. R. Swap, M. Garstang, S. Greco, R. Talbot, P. Kållberg, Saharan dust in the Amazon Basin. *Tellus B* **44**, 133–149 (1992).
2. M. J. Kennedy, O. A. Chadwick, P. M. Vitousek, L. A. Derry, D. M. Hendricks, Changing sources of base cations during ecosystem development, Hawaiian Islands. *Geology* **26**, 1015–1018 (1998).
3. O. A. Chadwick, L. A. Derry, P. M. Vitousek, B. J. Huebert, L. O. Hedin, Changing sources of nutrients during four million years of ecosystem development. *Nature* **397**, 491–497 (1999).
4. A. C. Kurtz, L. A. Derry, O. A. Chadwick, Accretion of Asian dust to Hawaiian soils: Isotopic, elemental, and mineral mass balances. *Geochim. Cosmochim. Acta* **65**, 1971–1983 (2001).
5. J. C. Pett-Ridge, Contributions of dust to phosphorus cycling in tropical forests of the Luquillo Mountains, Puerto Rico. *Biogeochemistry* **94**, 63–80 (2009).
6. M. A. McClintock, M. A. McClintock, G. Brocard, J. Willenbring, C. Tamayo, S. Porder, J. C. Pett-Ridge, Spatial variability of African dust in soils in a montane tropical landscape in Puerto Rico. *Chem. Geol.* **412**, 69–81 (2015).
7. R. C. Capo, O. A. Chadwick, Sources of strontium and calcium in desert soil and calcrete. *Earth Planet. Sci. Lett.* **170**, 61–72 (1999).
8. R. L. Reynolds, J. Belnap, M. C. Reheis, P. Lamothe, F. Luiszer, Aeolian dust in Colorado Plateau soils: Nutrient inputs and recent change in source. *Proc. Natl. Acad. Sci. U.S.A.* **98**, 7123–7127 (2001).
9. S. J. Van der Hoven, J. Quade, Tracing spatial and temporal variations in the sources of calcium in pedogenic carbonates in a semiarid environment. *Geoderma* **108**, 259–276 (2002).
10. R. L. Reynolds, J. Neff, M. C. Reheis, P. J. Lamothe, Atmospheric dust in modern soil on aeolian sandstone, Colorado Plateau (USA): Variation with landscape position and contribution to potential plant nutrients. *Geoderma* **130**, 108–123 (2006).
11. A. C. Reynolds, J. Quade, J. L. Betancourt, Strontium isotopes and nutrient sourcing in a semi-arid woodland. *Geoderma* **189–190**, 574–584 (2012).
12. A. A. Coble, S. C. Hart, M. E. Ketterer, G. S. Newman, A. L. Kowler, Strontium source and depth of uptake shifts with substrate age in semiarid ecosystems. *J. Geophys. Res. Biogeosci.* **120**, 1069–1077 (2015).
13. G. S. Okin, N. Mahowald, O. A. Chadwick, P. Artaxo, Impact of desert dust on the biogeochemistry of phosphorus in terrestrial ecosystems. *Global Biogeochem. Cycles* **18**, GB2005 (2004).
14. N. Mahowald, T. D. Jickells, A. R. Baker, P. Artaxo, C. R. Benitez-Nelson, G. Bergametti, T. C. Bond, Y. Chen, D. D. Cohen, B. Herut, N. Kubilay, R. Losno, C. Luo, W. Maenhaut, K. A. McGee, G. S. Okin, R. L. Siefert, S. Tsukuda, Global distribution of atmospheric phosphorus sources, concentrations and deposition rates, and anthropogenic impacts. *Global Biogeochem. Cycles* **22**, GB4026 (2008).
15. S. Myriokefalitakis, A. Nenes, A. R. Baker, N. Mihalopoulos, M. Kanakidou, Bioavailable atmospheric phosphorous supply to the global ocean: A 3-D global modeling study. *Biogeosciences* **13**, 6519–6543 (2016).
16. E. G. Green, W. E. Dietrich, J. F. Banfield, Quantification of chemical weathering rates across an actively eroding hillslope. *Earth Planet. Sci. Lett.* **242**, 155–169 (2006).
17. J. J. Owen, R. Amundson, W. E. Dietrich, K. Nishiizumi, B. Sutter, G. Chong, The sensitivity of hillslope bedrock erosion to precipitation. *Earth Surf. Proc. Land.* **36**, 117–135 (2011).
18. K. L. Ferrier, J. W. Kirchner, R. C. Finkel, Estimating millennial-scale rates of dust incorporation into eroding hillslope regolith using cosmogenic nuclides and immobile weathering tracers. *J. Geophys. Res.* **116**, F03022 (2011).
19. K. Soderberg, J. S. Compton, Dust as a nutrient source for fynbos ecosystems, South Africa. *Ecosystems* **10**, 550–561 (2007).
20. S. M. Aciego, C. S. Riebe, S. C. Hart, M. A. Blakowski, C. J. Carey, S. M. Aarons, N. C. Dove, J. K. Botthoff, K. W. W. Sims, E. L. Aronson, Dust outpaces bedrock in nutrient supply to montane forest ecosystems. *Nat. Commun.* **8**, 14800 (2017).
21. T. W. Walker, J. K. Syers, The fate of phosphorus during pedogenesis. *Geoderma* **15**, 1–19 (1976).
22. C. R. Lawrence, J. C. Neff, The contemporary physical and chemical flux of aeolian dust: A synthesis of direct measurements of dust deposition. *Chem. Geol.* **267**, 46–63 (2009).
23. S. Porder, S. Ramachandran, The phosphorus concentration of common rocks—A potential driver of ecosystem P status. *Plant Soil* 41–55 (2013).
24. E. W. Portenga, P. R. Bierman, Understanding Earth's eroding surface with ^{10}Be. *GSA Today* **21**, 4–10 (2011).
25. D. E. Granger, J. W. Kirchner, R. Finkel, Spatially averaged long-term erosion rates measured from in situ-produced cosmogenic nuclides in alluvial sediment. *J. Geol.* **104**, 249–257 (1996).
26. E. M. Clapp, P. R. Bierman, M. Caffee, Using ^{10}Be and ^{26}Al to determine sediment generation rates and identify sediment source areas in an arid region drainage basin. *Geomorphology* **45**, 89–104 (2002).
27. C. S. Riebe, D. E. Granger, Quantifying effects of deep and near-surface chemical erosion on cosmogenic nuclides in soils, saprolite, and sediment. *Earth Surf. Proc. Land.* **38**, 523–533 (2013).
28. S. Albani, N. M. Mahowald, A. T. Perry, R. A. Scanza, C. S. Zender, N. G. Heavens, V. Maggi, J. F. Kok, B. L. Otto-Bliesner, Improved dust representation in the Community Atmosphere Model. *J. Adv. Model. Earth Syst.* **6**, 541–570 (2014).
29. S. Albani, N. M. Mahowald, G. Winckler, R. F. Anderson, L. I. Bradtmiller, B. Delmonte, R. François, M. Goman, N. G. Heavens, P. P. Hesse, S. A. Hovan, S. G. Kang, K. E. Kohfeld, H. Lu, V. Maggi, J. A. Mason, P. A. Mayewski, D. McGee, X. Miao, B. L. Otto-Bliesner, A. T. Perry, A. Pourmand, H. M. Roberts, N. Rosenbloom, T. Stevens, J. Sun, Twelve thousand years of dust: The Holocene global dust cycle constrained by natural archives. *Clim. Past* **11**, 869–903 (2015).
30. J. D. Pelletier, J. P. Cook, Deposition of playa windblown dust over geologic time scales. *Geology* **33**, 909–912 (2005).
31. P. M. Vitousek, M. J. Kennedy, L. A. Derry, O. A. Chadwick, Weathering versus atmospheric sources of strontium in ecosystems on young volcanic soils. *Oecologia* **121**, 255–259 (1999).
32. S. M. Aciego, B. Bourdon, M. Lupker, J. Rickli, A new procedure for separating and measuring radiogenic isotopes (U, Th, Pa, Ra, Sr, Nd, Hf) in ice cores. *Chem. Geol.* **266**, 194–204 (2009).
33. R. H. Whittaker, *Communities and Ecosystems* (MacMillan Publishing Co. Inc., 1975).
34. W. J. Hahm, C. S. Riebe, C. E. Lukens, S. Araki, Bedrock composition regulates mountain ecosystems and landscape evolution. *Proc. Natl. Acad. Sci.* **111**, 3338–3343 (2014).
35. N. M. Mahowald, D. R. Muhs, S. Levis, P. J. Rasch, M. Yoshioka, C. S. Zender, C. Luo, Change in atmospheric mineral aerosols in response to climate: Last glacial period, preindustrial, modern, and doubled carbon dioxide climates. *J. Geophys. Res.* **111**, D10202 (2006).
36. J. A. Wald, R. C. Graham, P. J. Schoeneberger, Distribution and properties of soft weathered bedrock at ≤ 1 m depth in the contiguous United States. *Earth Surf. Proc. Land.* **38**, 614–626 (2013).
37. J. W. Kirchner, R. C. Finkel, C. S. Riebe, D. E. Granger, J. L. Clayton, J. G. King, W. F. Megahan, Mountain erosion over 10 yr, 10 k.y., and 10 m.y. time scales. *Geology* **29**, 591–594 (2001).
38. C. T. Hunsaker, D. G. Neary, Sediment loads and erosion in forest headwater streams of the Sierra Nevada, California. *25th General Assembly Int. Union Geodesy Geophys.* **353**, 195–203 (2012).
39. C. S. Riebe, W. J. Hahm, S. L. Brantley, Controls on deep critical zone architecture: A historical review and four testable hypotheses. *Earth Surf. Proc. Land.* **42**, 128–156 (2017).
40. L. P. Gromet, L. T. Silver, Rare earth element distributions among minerals in a granodiorite and their petrogenetic implications. *Geochim. Cosmochim. Acta* **47**, 925–939 (1983).
41. E. B. Watson, T. H. Green, Apatite/liquid partition coefficients for the rare earth elements and strontium. *Earth Planet. Sci. Lett.* **56**, 405–421 (1981).
42. J. F. Banfield, R. A. Eggleton, Apatite replacement and rare earth mobilization, fractionation and fixation during weathering. *Clays Clay Miner.* **37**, 113–127 (1989).
43. H. Nagasawa, Rare earth concentrations in zircons and apatites and their host dacites and granites. *Earth Planet. Sci. Lett.* **9**, 359–364 (1970).
44. D. Lal, Cosmic ray labeling of erosion surfaces: In situ nuclide production rates and erosion models. *Earth Planet. Sci. Lett.* **104**, 424–439 (1991).
45. D. E. Granger, C. S. Riebe, in *Treatise on Geochemistry*, J. I. Drever, Ed. (Elsevier, ed. 2, 2014), vol. 7, pp. 401–436.
46. G. Balco, J. O. Stone, N. A. Lifton, T. J. Dunai, A complete and easily accessible means of calculating surface exposure ages or erosion rates from ^{10}Be and ^{26}Al measurements. *Quat. Geochronol.* **3**, 174–195 (2008).
47. E. E. Small, R. S. Anderson, G. S. Hancock, Estimates of the rate of regolith production using ^{10}Be and ^{26}Al from an alpine hillslope. *Geomorphology* **27**, 131–150 (1999).
48. C. S. Riebe, J. W. Kirchner, D. E. Granger, Quantifying quartz enrichment and its consequences for cosmogenic measurements of erosion rates from alluvial sediment and regolith. *Geomorphology* **40**, 15–19 (2001).
49. J. L. Dixon, A. M. Heimsath, R. Amundson, The critical role of climate and saprolite weathering in landscape evolution. *Earth Surf. Proc. Land.* **34**, 1507–1521 (2009).
50. A. M. Heimsath, R. A. DiBiase, K. X. Whipple, Soil production limits and the transition to bedrock-dominated landscapes. *Nat. Geosci.* **5**, 210–214 (2012).
51. K. Nishiizumi, M. Imamura, M. W. Caffee, J. R. Southon, R. C. Finkel, J. McAninch, Absolute calibration of ^{10}Be AMS standards. *Nucl. Instrum. Methods Phys. Res. B.* **258**, 403–413 (2007).

52. C. S. Riebe, J. W. Kirchner, R. C. Finkel, Erosional and climatic effects on long-term chemical weathering rates in granitic landscapes spanning diverse climate regimes. *Earth Planet. Sci. Lett.* **224**, 547–562 (2004).
53. S. M. Mudd, M.-A. Harel, M. D. Hurst, S. W. D. Grieve, S. M. Marrero, The CAIRN method: Automated, reproducible calculation of catchment-averaged denudation rates from cosmogenic nuclide concentrations. *Earth Surf. Dynam.* **4**, 655–674 (2016).
54. C. P. Kohl, K. Nishiizumi, Chemical isolation of quartz for measurement of in-situ-produced cosmogenic nuclides. *Geochim. Cosmochim. Acta* **56**, 3583–3587 (1992).
55. Purdue University Department of Physics, Purdue Rare Isotope Measurement Laboratory (2017); available at www.physics.purdue.edu/primelab/.
56. P. Muzikar, D. Elmore, D. E. Granger, Accelerator mass spectrometry in geologic research. *Geol. Soc. Am. Bull.* **115**, 643–654 (2003).
57. D. E. Granger, A. L. Smith, Dating buried sediments using radioactive decay and muogenic production of ^{26}Al and ^{10}Be. *Nucl. Instrum. Methods Phys. Res. B.* **172**, 822–826 (2000).
58. California Department Water Resources, California Data Exchange Center (2013); available at http://cdec.water.ca.gov.
59. J. Kellndorfer, W. Walker, K. Kirsch, G. Fiske, J. Bishop, L. LaPoint, M. Hoppus, J. Westfall, "NACP Aboveground Biomass and Carbon Baseline Data (NBCD 2000), U.S.A., 2000" (ORNL DAAC, 2012); available at http://dx.doi.org/10.3334/ORNLDAAC/1081.
60. P. J. Patchett, M. Tatsumoto, A routine high-precision method for Lu-Hf isotope geochemistry and chronology. *Contrib. Mineral. Petrol.* **75**, 263–267 (1981).
61. J. Blichert-Toft, N. T. Arndt, G. Gruau, Hf isotopic measurements on Barberton komatiites: Effects of incomplete sample dissolution and importance for primary and secondary magmatic signatures. *Chem. Geol.* **207**, 261–275 (2004).
62. T. J. Lapen, N. J. Mahlen, C. M. Johnson, B. L. Beard, High precision Lu and Hf isotope analyses of both spiked and unspiked samples: A new approach. *Geochem. Geophys. Geosyst.* **5**, Q01010 (2004).
63. S. M. Aciego, K. M. Cuffey, J. L. Kavanaugh, D. L. Morse, J. P. Severinghaus, Pleistocene ice and paleo-strain rates at Taylor Glacier, Antarctica. *Quaternary Res.* **68**, 303–313 (2007).
64. S. M. Aarons, S. M. Aciego, J. D. Gleason, Variable Hf-Sr-Nd radiogenic isotopic compositions in a Saharan dust storm over the Atlantic: Implications for dust flux to oceans, ice sheets and the terrestrial biosphere. *Chem. Geol.* **349–350**, 18–26 (2013).
65. S. B. Jacobsen, G. J. Wasserburg, Sm-Nd isotopic evolution of chondrites. *Earth Planet. Sci. Lett.* **50**, 139–155 (1980).
66. J. S. Lackey, M. R. Cecil, C. J. Windham, R. E. Frazer, I. N. Bindeman, G. E. Gehrels, The Fine Gold Intrusive Suite: The roles of basement terranes and magma source development in the Early Cretaceous Sierra Nevada batholith. *Geosphere* **8**, 292–313 (2012).

Acknowledgments: We thank R. Callahan for data analysis and field work, L. Sklar for insightful discussion, and N. Mahowald for help in accessing model data. **Funding:** This material is based on work supported by the NSF Graduate Research Fellowship under grant no. DGE-1252375 to L.J.A. C.S.R. acknowledges funding from NSF grants EPS 1208909 and EAR 1331939. S.M.A. acknowledges support from the David and Lucile Packard Foundation. **Author contributions:** L.J.A. and C.S.R. contributed equally to study design and paper writing. L.J.A. collected the samples, helped prepare samples for analysis, combined the global data sets, conducted the data analysis, and created all figures. S.M.A. contributed to the study design, provided materials and methods, conducted the Nd analyses, and contributed to writing the paper. M.A.B. prepared samples and contributed to writing the Materials and Methods section. **Competing interests:** The authors declare that they have no competing interests. **Data and materials availability:** All data reported in the paper can be found in the supplementary tables. LGM and modern dust deposition models (*28*) are available at www.geo.cornell.edu/eas/PeoplePlaces/Faculty/mahowald/dust/albanietal2014/Shared%20data/. We used the Albanietal2014_C4fn-lgm_dep.nc and Albanietal2014_C4fn_dep.nc data sets for LGM and modern dust deposition rates, respectively. The global database of ^{10}Be-based erosion rates (*24*) is available as Geological Society of America supplemental data item 2011216. ^{10}Be concentrations for southern Sierra Nevada catchments D102, P301, P303, and P304 are available in supplementary file Dataset_S01 from the work of Hahm *et al*. (*34*). The sediment yield data that we used for 30 Idaho catchments are presented in table 1 of the study of Kirchner and others (*37*). The sediment yield data that we used for eight Sierra Nevada catchments are presented in table 1 of the study of Hunsaker and Neary (*38*). Last, Nd isotope data for southern Sierra Nevada dust samples are available from table S1 of the study of Aciego *et al*. (*20*).

Submitted 20 June 2017
Accepted 9 November 2017
Published 6 December 2017
10.1126/sciadv.aao1588

Citation: L. J. Arvin, C. S. Riebe, S. M. Aciego, M. A. Blakowski, Global patterns of dust and bedrock nutrient supply to montane ecosystems. *Sci. Adv.* **3**, eaao1588 (2017).